Accepted Manuscript

Bifunctional biomass-derived N, S dual-doped ladder-like porous carbon for supercapacitor and oxygen reduction reaction

Donglin He, Wang Zhao, Ping Li, Sen Sun, Qiwei Tan, Kun Han, Luan Liu, Lang Liu, Xuanhui Qu

PII: S0925-8388(18)33381-4

DOI: 10.1016/j.jallcom.2018.09.141

Reference: JALCOM 47560

To appear in: *Journal of Alloys and Compounds*

Received Date: 17 June 2018

Revised Date: 11 September 2018

Accepted Date: 12 September 2018

Please cite this article as: D. He, W. Zhao, P. Li, S. Sun, Q. Tan, K. Han, L. Liu, L. Liu, X. Qu, Bifunctional biomass-derived N, S dual-doped ladder-like porous carbon for supercapacitor and oxygen reduction reaction, *Journal of Alloys and Compounds* (2018), doi: https://doi.org/10.1016/j.jallcom.2018.09.141.

Bifunctional biomass-derived N, S dual-doped ladder-like porous carbon for supercapacitor and oxygen reduction reaction

Donglin He,[a] Wang Zhao,[a] Ping Li,[*abc] Sen Sun,[a] Qiwei Tan,[a] Kun Han,[a] Luan Liu,[a] Lang Liu,[d] and Xuanhui Qu[*ace]

[a] Institute for Advanced Materials and Technology, University of Science and Technology Beijing, Beijing 100083, China

[b] Beijing Key Laboratory for Advanced Powder Metallurgy and Particulate Materials, University of Science and Technology Beijing, Beijing 100083, China

[c] Beijing Laboratory of Metallic Materials and Processing for Modern Transportation, University of Science and Technology Beijing, Beijing 100083, China

[d] School of Chemical Engineering, The University of Queensland, Brisbane, QLD, 4072, Australia

[e] The State Key Laboratory for Advanced Metals and Materials, University of Science and Technology Beijing, Beijing 100083, China

* Corresponding author

Email address: ustbliping@126.com (Prof. Ping Li); quxh@ustb.edu.cn (Prof. Xuanhui Qu)

ABSTRACT

In recent years, heteroatom-doped biomass-derived carbon has attracted intensive attention in vast fields due to their inexpensive precursors and abundant resources, especially in oxygen reduction reaction and supercapacitors. This research demonstrates a simple strategy to prepare mulberry leaves-derived nitrogen, sulfur dual-doped ladder-like porous carbon material, which possesses high content of nitrogen (8.17 at %), sulfur (1.97 at %),

large surface area (1689 m^2 g^{-1}) and porous structure with a mass of micropores and mesopores. With respect to electrode material of supercapacitor, the nitrogen, sulfur dual-doped ladder-like carbon exhibits large specific capacitance of 243.4 F g^{-1} at 0.1 A g^{-1} and outstanding durability (94 % retention after 5000 cycles at 3 A g^{-1}). Moreover, in comparison to Pt/C catalyst, nitrogen, sulfur dual-doped ladder-like porous carbon presents excellent electrochemical performances of long term stability (90.2% retention after 20000 s) and resistance to methanol crossover for oxygen reduction reaction. This work successfully may provide a new case to take advantage of nature materials to fabricate heteroatom-doped carbon for energy conversion and storage.

Keywords: N,S dual-doping; Bifunctional biomass-derived carbon; Supercapacitor; Oxygen reduction reaction

1. Introduction

With the development of economy, energy crisis and environmental impact are becoming increasingly severe, increasing a sustainable need to discover renewable energy resources and develop energy devices [1], such as fuel cell and supercapacitor (SC) [2]. Catalysts are the key materials in fuel cell. Nonetheless, the high price and scarcity of typical platinum catalyst for oxygen reduction reaction (ORR) hamper scale applications of fuel cells [3]. So intensive efforts have been made to investigate nonprecious metal and metal-free catalysts [4]. SCs have excellent cycling ability and high power/energy density, which are mostly determined by active materials [5].

Carbon materials, such as graphene [6-8], CNTs [9-11], carbon aerogels [12] and active carbon [13] have been extensively studied in energy fields as EDLCs electrode materials and

ORR catalysts. To enhance the property of carbon materials, heteroatom (N,S,P,B,*etc.*) doping is used as an effective and important method, which is benefitial to decrease charge transfer resistance and improve wettability [14]. Recently, heteroatom-doped carbon materials, for example, N-doped porous carbon [15-20], S, N co-doped carbon nanosheets [21-23], N, S co-doped 3D honeycomb-like carbon [24] and N and S co-doped biomass-derived carbon [14, 25], have been widely researched for ORR catalysts and electrode materials of SCs. Among them, due to the abundance, low expense, and the recyclability, biomass-derived carbon is an attractive candidate, typically, rice straw-derived porous carbon for SC [26], porous carbon from banana fibers for SC [27], potato residue -derived N-doped porous carbon for SC [28], N-doped mesoporous carbon from chin for ORR [29], N-doped nanoporous carbon from typha orientalis for ORR [30], N-doped carbon from microorganism for ORR and SC [31]. Nonetheless, these investigations mostly focused on single energy application (ORR or SC). Therefore, developing multifunctional biomass-derived heteroatom-doped carbon is desirable.

There is much effort focusing on utilizing biomass to fabricate energy storage devices, but little attention has been paid on mulberry leaves, which will be investigated to use for ORR and SCs for the first time. Herein, we demonstrate a straightforward, inexpensive and readily scalable method to prepare nitrogen, sulfur dual-doped ladder-like porous carbon (NSLPC) by pretreatment of activation with KOH and postprocessing of doping with thiourea. The method has three advantages as follow: (1) a sustainable biomass, mulberry leaves, is used as the carbon source; (2) facile preparation method with no templates are needed, and it is worth noting that a unique ladder-like porous carbon is obtained from the natural structure

of the mulberry leaves; (3) the resultant NSLPC possesses numerous mesopores and micropores, large specific surface area (SSA), high level of N. Based on the aforementioned features, the NSLPC sample presents high specific capacitance (243.4 F g^{-1} at 0.1 A g^{-1}) and excellent durability (94% retention after 5000 cycles at 3 A g^{-1}) for SCs in 6 M KOH solution. Moreover, the NSLPC shows near four-electron pathway, resistance to methanol poisoning and high stability for ORR. This reproducible biomass material, simple synthetic method, and outstanding property make NSLPC a potential candidate for ORR catalyst in fuel cells and electrode material in SCs.

2. Experimental

2.1. Materials

Mulberry leaves (MLs) were collected in Sichuan, China. Ethanol absolute, thiourea, urea, 37 wt % hydrochloric acid (HCl) and 5 wt % nafion solution were bought from Sinopharm Group. The commercial Pt/C catalysts (20 wt%) were provided by Johnson Matthey Company.

2.2. Synthesis

Mulberry leaves, washed repeatedly by DI water, were baked overnight in drying oven at 90 °C and ground into powder. Then the dried mulberry leaves powder mixed with KOH (mass ratio of 1:4) were transferred into tube furnace, heated to 800 °C and pyrolyzed in Ar flow for 2 h. After the temperature cooled down to room temperature, the pyrolytic material was immersed in 2 mol L^{-1} HCl for 24 h, repeatedly washed by DI water and ethanol to completely eliminate any residues of metal and then freeze-dried to gain mulberry leaves-derived ladder-like porous carbon (LPC). The thiourea and LPCs (mass ratio of 4:1)

were mixed in a mortar with pestle for 0.5 h, and the mixture was placed into the corundum tube for pyrolyzation at 800 °C for 1 h with shielding atmosphere of argon. The obtained products were denoted as NSLPC.

At the same time, for comparison, nitrogen doped mulberry leaves-derived ladder-like porous carbon (NLPC) was synthesized with urea used doping agent in the same way.

2.3. Characterization

The morphology of produced carbon materials were observed by scanning electron microscope (SEM, SU8010), transmission electron microscopy (TEM, JEOL, JEM-2010). Element mapping images were acquired by the SU8010 with energy-dispersive X-ray spectrometry (EDS) system. The crystal structure analysis was carried out on X-ray diffraction (XRD, Cu Kα radiation, λ=1.5406 Å), 2θ angle ranging from 10º to 90º. N_2 adsorption-desorption isotherms were test at 77K via Micromeritics ASAP 2460 Surface Area and Porosimetry analyzer analyzer after the products were pretreated in a vacuum at 200 °C. The SSA and pore size distributions (PSD) were conducted through Brunauer-Emmett-Teller (BET) method and a density functional theory (DFT), respectively. X-ray photoelectron spectra (XPS) were recorded with a Kratos AXIS spectrometer with a monochromic Al Kα (hν =1486.69 eV) radiation. Raman spectra of prepared samples were recorded with a LabRAM HR Evolution instrument.

2.4. Electrochemical measurement

2.4.1 Electrochemical characterizations for supercapacitors

The electrochemical performances of supercapacitors were measured by an electrochemical workstation (Chenhua CHI760E). To obtain the working electrodes, typically,

the mixture containing the acetylene black (10 wt %), products (80 wt %) and polytetrafluoroethylene (PTFE) binder (10 wt %) was coated onto a current collector of Ni foam with 10 MPa, followed by drying overnight. The platinum foil and Hg/HgO electrode acted as the counter electrode and reference electrode, respectively. The electrolyte is 6.0 mol L^{-1} KOH solution.

Cyclic voltammetry (CV), electrochemical impedance spectroscopy (EIS) and galvanostatic charge/discharge (GCD) curves were recorded with CHI760E electrochemistry workstation. The stability experiment was performed at 3 A g^{-1} by Land cell tester. The capacitance was determined by the follow equations:

$$C_g = \frac{I \times \Delta t}{m \times \Delta V} \quad (1)$$

Where C_g (F g^{-1}), I (mA), Δt (s), m (mg) and V (V) denote the specific discharge capacitance, working current, discharge time, mass of electrode active materials and potential, respectively.

2.4.2 Electrochemical measurement for ORR

In addition, the electrochemical measurements for ORR were tested on CHI760E workstation with a three-electrode cell. Saturated calomel electrode (SCE) with a salt bridging and platinum foil (1 cm^2) were employed as the reference electrode and counter electrode, respectively. Rotation disk electrode (RDE, diameter of 5 mm) modified by catalysts acted as the working electrode. In order to prepare working electrode, the synthesized carbon (2 mg) was added into a mixture of ethanol (800 μL), DI water (100 μL) and Nafion solution (100 μL), and the mixture was sonicated for about 0.5h to get a homogeneous ink. 20 μL catalyst ink was dropped to the surface of the glass carbon disk,

followed by drying to get a catalyst film, obtaining a mass loading of 0.204 mg cm^{-2}. As a contrast, the Pt/C catalyst was coated on the glass carbon disk surface with a similar method. All the potential values mentioned for ORR are revised by reversible hydrogen electrode (RHE).

Linear sweep voltammetry (LSV) and CV were performed in 0.1 mol L^{-1} KOH saturated with O_2 at 10 mV s^{-1}. The electrochemical stability and crossover effect were tested by current-time chronoamperometric response at 0.7 V with continuous O_2 bubbling, respectively. The electron number (n) was computed by Koutecky-Levich (K-L) equations:

$$\frac{1}{J}=\frac{1}{J_{\mathrm{k}}}+\frac{1}{B\omega^{1/2}} \quad (2)$$

$$B=0.2nFC_O D_O^{2/3}\nu^{-1/6} \quad (3)$$

Where J, J_k ω and n stand the measured current density, kinetic-limiting current density, the electrode rotation speed in rpm, the overall electron transfer number, respectively, F is the Faradaic constant (96485C mol^{-1}), C_O is the O_2 saturation concentration in 0.1 M KOH (1.2×10^{-6} mol cm^{-3}), ν is the kinematic viscosity of the 0.1M KOH (1.13×10^{-2} cm^2 s^{-1}), and D_O is the O_2 diffusion coefficient in 0.1 M KOH (1.9×10^{-5} cm^2 s^{-1}). The 0.2 is a constant when the rotation rate is denoted in rpm.

3. Results and discussions

3.1 Preparation

As exhibited in Scheme 1, the mulberry leaves-derived N, S dual-doped ladder-like porous carbon materials were prepared by chemical activation method using KOH as a activator and thiourea as a doping agent. After washed by distilled water and dried, the taro stems mixed with KOH were carbonized at 800 °C. After that the products of LPC were

washed in 2 M HCl solution and freeze-dried. Further, the mixture of the LPC and thiourea was pyrolyzed to prepare the N, S co-doped ladder-like porous carbon at 800 °C for 1 h. The N, S co-doped ladder-like porous carbon material is denoted as NSLPC. It is noted that this synthesis method demonstrates a path to utilize biomass to easily produce multifunctional porous materials for electrochemical energy storage system.

3.2 Structural characterization

Fig.1 shows typical morphology of the NSLPC samples. The SEM images of NSLPC samples at different magnifications present an unique ladder-like and interconnected structure with a little fragments (Fig. 1a and 1b), which maybe comes from the inherent microstructure of mulberry leaves. And this particular ladder-like morphology may be good for structural stability. Similar structures can be observed for LPC and NLPC shown in Fig. S1. EDS element mapping images visually exhibit that the carbon, nitrogen, sulfur and oxygen heteroatoms are uniformly distributed throughout the NSLPC framework structures (Fig.1c and 1d). Typical TEM images of the NSLPC material are displayed in Fig. 1e-1g. Fig. 1e clearly shows the low-magnification TEM image, which exhibits tiny porous structure attributed to KOH activation and the emissions of water and carbon dioxide at high temperature [32]. High-resolution TEM image (Fig.1f) does not exhibit any crystalline lattice fringes, which is in accordance with SAED result (Fig. 1g), demonstrating the nature of amorphous carbon.

The crystalline phase of LPC, NLPC and NSLPC were performed by XRD. There are two wide characteristic diffraction peaks at 23° and 44° from the XRD patterns of these three samples (Fig.2a), in accordance with the (002) and (100) lattice planes of graphite,

respectively. Differently, the intensity of the diffraction peak in NLPC and NSLPC is higher than these in LPC, indicating the better degree of graphitization for NLPC and NSLPC, which is mainly contributed to the high temperature doping at 800 □. The structures of LPC, NLPC and NSLPC were characterized by Raman spectrums. As plotted in Fig. 2b, raman spectrums of LPC, NLPC and NSLPC display two remarkable peaks at 1346 and 1596 cm^{-1}, which are assigned to graphitic sp^2 (G band) and disordered sp^3 carbon (D band), respectively. As an indicator of the level of disordering and the graphitic degree of the carbon materials, the intensity ratio of the D and G band (I_D/I_G) is adopt. I_D/I_G intensity ratios calculated from the spectra of LPC, NLPC and NSLPC are 1.07, 1.05 and 1.02, respectively. The relatively lower I_D/I_G intensity ratio of NSLPC sample confirms a decrease in the disordered structure and the higher degree of graphitization. This result can match with the XRD result.

N_2 adsorption-desorption isothermal curves were recorded to study the SSA and porosity of the resultant LPC, NPLC and NSLPC samples. Fig.2c shows the typical three N_2 adsorption-desorption isothermal curves, which presents similar trend. From the adsorption isotherm of LPC, NPLC and NSLPC samples, nitrogen adsorption at a low pressure ($P/P_0 <$ 0.01) indicates the filling of luxuriant micropores. Besides, these three N_2 adsorption-desorption isothermal curves could be classified as a combined type I and IV with a clear hysteresis loop of the type H4 on the basis of the IUPAC [33]. It is noted that the H4 hysteresis loop appears at a wide relative pressure (0.45~1.0 P/P_0), indicating the existence of abundant mesopores. The pore size distribution of LPC, NLPC and NSLPC are further calculated by DFT method, as exhibited in Fig. 2d. Particularly, distinct peaks are located at about 0.5 nm, 0.8nm and 1.3nm in the PSD, indicating the existence of ultramicropores [34],

micropores along with mesopores and macropores (>2 nm). It is reported that the ultramicropore is helpful for the electrochemical performances for SCs [35-38]. Moreover, a wide pore distribution within 2.3~10 nm, mesoporous, also occurred. Particularly, the SSA, total pore volumes, micropore and meso/macropore volumes of these carbon materials are listed in Table 1. Specifically, the SSAs of LPC, NLPC and NSLPC calculated by BET method are 568, 1207, 1689 $m^2 g^{-1}$, and the total pore volumes are 0.31, 0.72 and 1.01 $cm^3 g^{-1}$, respectively. It is found that the $V_{meso+macro}$ of NSLPC (0.655 $cm^3 g^{-1}$) is larger than that of LPC (0.106 $cm^3 g^{-1}$) and NLPC (0.399 $cm^3 g^{-1}$). At the same time, the $V_{meso+macro}$ of NSLPC (0.655 $cm^3 g^{-1}$) is larger than the V_{micro} (0.357 $cm^3 g^{-1}$), demonstrating that the NSLPC has also abundant mesopores and macropores. And the average pore diameter of NSLPC is 2.39 nm. It is clearly observed that the SSA of NSLPC is much higher than that of LPC and NLPC, which is ascribed to the addition of doping agent that play a role as self-porogen with the elimination of generated gas [39]. After all, the NSLPC has high SSA and wide range of PSD comprising of the micropores and mesopores, which is of great benefit to catalysis and SCs. The ladder-like porous structures not only boost electrochemical performance in where the high mass transport rate of ion is achieved, but also has great importance to the electric double-layer capacity because of their high specific surface area. Hence, porous carbon is ideal for the production of double-layer supercapacitor and catalyst.

Surface chemical compositions of these samples are further investigated by XPS. There are four representative peaks of C 1s (284.7 eV), N 1s (398.6 eV), O 1s (532.9 eV) and S 2p (164.1 eV) in the survey spectra of NSLPC samples (Fig. 3a), confirming that nitrogen and sulfur species have been incorporated into the carbon framework of NSLPC. Besides, no

other peaks are seen in the spectrum, demonstrating the complete removal of all the other trace elements, in accordance with the results of XRD. Additionally, according to the integrated peak areas of XPS data, the detailed atomic percentages of LPC, NLPC and NSLPC are calculated and summarized in Table 1. Particularly, the atomic percentage contents of carbon, nitrogen, sulfur and oxygen for NSLPC sample is 82.53 at %, 8.17 at %, 1.97 at %, and 7.34 at %, respectively. However, the XPS spectra of LPC and NLPC have no peaks of S 2p, and the N atomic percentage of NLPC is not much different from that of NSLPC. As shown in Fig.3b, these three component peaks of C1s for NSLPC locate at 284.7, 285.4 and 288.7 eV, which are ascribable to the bonds of sp^2 C=C, sp^3 C-C and C=O/C=N/C=S bonds, respectively [40-42]. The fitted N1s high resolution spectrum is exhibited in Fig. 3c. It is clerly seen that three individual peaks appear at 398.5, 400.4 and 401.3 eV, representing pyridinic N, pyrrolic N and graphitic N [43], respectively. In addition, as plotted in Fig. 3d, this fitted high resolution spectra of S 2p also presents three peaks, which are located at 163.9, 165.15 and 167.3 eV. The peak at 167.3 eV may be corresponded to -C-SOx-C- sulfone bridges (31%) that make no difference to ORR [44], as shown in Fig.3e. The other two peaks at 163.9 and 165.15 eV are assigned to the spin–orbit coupling of C-S-C 2p 3/2 and C-S-C 2p 1/2 bond , respectively [25], which are derived from thiophene-S (68.8%). It is reported that thiophene-like S can enhance conductivity [45]. The surface contents of different element species for NSLPC sample are shown in Fig. 3e. Combined with the XPS spectra and the results from a previous report [46], the possible schematic model for the chemical structure of NSLPC doped with both N and S is shown in Fig. 3f. Overall, the

above results confirm that the N and S species have been successfully incorporated into the carbon lattice of NSLPC.

3.3 Electrochemical performance of Supercapacitor

CV, GCD and EIS were test to study the electrochemical performance of LPC, NLPC and NSLPC in a three-electrode cell with 6 mol L^{-1} KOH as the electrolyte. The typical CVs of LPC (Fig. S2a), NLPC (Fig. S2b) and NSLPC (Fig. 4a) electrode were recorded with a scan speed from 5 to 100 mV s^{-1} at potential range between -1 and 0 V. Distinctly, the CV curves of NSLPC exhibit regular rectangular shape at low scan speed, indicating to be the representative characteristic of electrical double layer capacitor behavior (EDLC), demonstrating quick ion transport in NSLPC electrode materials. However, the CV curves show a near rectangular shape and a slight deviation at a relative high scan rate, which is ascribable to some pseudocapacitive effects because of the nitrogen, sulfur and oxygen functional groups [33, 47, 48]. The incorporated sulfur species into the carbon framework could influence the surface charge and offer up pseudocapacitive effect [49]. Meanwhile, the doping of N into carbon framework can improve the conductivity and wettability, and offer up a pseudocapacitance [50]. Besides, the oxygen species doped into carbon framework may improve the wettability of electrode interface, and contribute affluent faradic pseudocapacitance in aqueous electrolytes [51]. According to the GCD profiles in Fig.4b, NSLPC shows a capacitance of 214.5 F g^{-1} at 0.5 A g^{-1}, which is much higher than that of NLPC (185.5 F g^{-1} at 0.5 A g^{-1}) and LPC (165 F g^{-1} at 0.5 A g^{-1}). As shown in Fig. 4c, the capacitive performance of NSLPC electrode was further performed by galvanostatic experiments at 0.1 to 20 A g^{-1}. It is observed that the GCD curves of the NSLPC exhibit the symmetrical, linear and

triangular characteristics with a little IR drop, demonstrating good capacitive behaviors of EDLC. Simultaneously, the GCD curves of LPC and NLPC electrode are shown in Fig. S2c-d, which were tested at 0.1 to 20 A g^{-1}. Further, Fig.4d sums up the specific capacitance of the LPC, NLPC and NSLPC on the basis of the GCD measurements from 0.1 to 20 A g^{-1}. It is obvious that the NSLPC possesses the highest capacitance in comparison to NLPC and LPC at the tested current densities. Particularly, the detailed specific capacitances of NSLPC are 243.4, 223.4 and 206.8 F g^{-1} at 0.1, 0.2 and 1 A g^{-1}, respectively, which is superior to pine tree-derived carbon [52]. Even at a current density of 10 A g^{-1}, the specific capacitance reaches up to 168 F g^{-1}, which is higher than chitosan-derived aerogels [53], and the detailed comparison is summarized in Table 2.

The outstanding capacitive performance of NSLPC may be ascribed to its high SSA, much more porous structure and synergistic effect of N,S co-doping compared to NLPC and LPC. Simultaneously, doping of N and S with the presence of O efficiently augments the capacitance of carbon material [47]. It is reported that the pyridinic N and pyrrolic N generally are good for the pseudocapacitance, while graphitic N can enhance the conductivity of the carbon material [59, 60]. Likewise, doped S species could heighten surface property of the carbon material, which is benificial to pseudocapacitance [61]. Cycling durability is an extremely crucial aspect to the practical application of SC. Therefore, the cycling stability of NSLPC was tested by GCD at 3 A g^{-1} for 5000 cycles. As plotted in Fig. 4e, the GCD curves of NSLPC show that the capacitance retention is still beyond 94% after 5000 cycles, demonstrating its outstanding long cycling stability. In general, good stability is partially ascribed to double layer charge-discharge process in the electrode materials. As shown in Fig. 4f, the EIS spectrum presents that the as-fabricated NSLPC electrode has an almost vertical curve in the low frequency region, demonstrating a good capacitive behavior. The successful

doping of N and S species enhance the surface polarity and wettability with electrolyte, which is good to decrease the charge-transfer resistance. Meanwhile, the semi-circle is very small in the high frequency region, indicating a little internal resistance.

3.4 Electrochemical performance of ORR

ORR catalytic activity of these samples was tested by CV measurements in nitrogen- and oxygen-saturated electrolyte solution. To evaluate the possibility of the practical requirements for NSLPC, the commercial Pt/C catalyst was tested under the same condition as a comparison. As exhibited in Fig. 5a (solid line), quasi-rectangular double-layer capacitive backgrounds in 0.1 M KOH solution saturated with nitrogen are clearly observed without no redox peak. On the contrary, the NSLPC catalyst displays a strong O_2 reduction peak at +0.86V in electrolyte solution saturated with O_2, which is more positive than that of NLPC (+0.84V) and LPC (+0.71V), implying that O_2 is more easy to be reduced on the NSLPC catalyst [62]. Consequently, the NSLPC sample demonstrates to be the optimal catalytic performance among the three samples investigated in terms of the peak potential, surface area and active.?? Subsequently, the adsorption of oxygen molecules on the adjacent C atoms is enhanced and the O-O chemical bonds are weakened [63].

LSV curves were used to further evaluate the activity of as-obtained materials and the kinetics for ORR process. Fig. 5b presents a set of LSV curves with different rotating speed for NSLPC. It is observed that the ORR current densities increase with the increase of rotation rate due to the shortened diffusion distance, and the current density reaches diffusion limiting current density at each rotation rate. As shown in Fig. S3, the onset potential of the NSLPC is about 0.86 V, which is comparable to that of commercial Pt/C (0.88). Though the

limiting current density of the NSLPC is lower than that of the Pt/C catalyst. As plotted in Fig. 5c, the corresponding K-L curves show excellent correlation between $\omega^{-0.5}$ and J^{-1}. Meanwhile, the excellent linear relationship of K-L curves suggest that a similar electron transfer at different potentials. Calculated from the slope of the K-L curves, the electron transfer number is about 3.7~3.9, demonstrating a near 4-electron pathway within the ORR process. This result further confirms that NSLPC sample has a good catalytic activity.

Methanol crossover is quite important for practical application in fuel cells. The chronoamperometric responses were tested for NSLPC and Pt/C catalyst with addition of CH_3OH, assessing the selectivity for catalyst at 900 rpm. As shown in Fig. 5d, the current density of the NSLPC electrode displays negligible decrease after the 3 M methanol is added at 300 s, demonstrating an outstanding catalytic selectivity. By contrast, the current density of Pt/C catalyst suffers a dramatic decrease along with methanol oxidation reaction (MOR) [64]. As a critical factor for ORR catalyst performance, stability plays an important role in long-term life for practical applications. As shown in Fig. 5e, the stability performance of NSLPC for ORR exhibits a high retention of 90.2% after 20000 s, distinguished from that 83% for Pt/C under the same experimental condition. The result shows that the NSLPC catalyst with good selectivity and excellent long-term stability has potential as a electrocatalyst for ORR.

The EIS measurements were adopted to study electrical resistance and ion transport behavior for ORR. The representative Nyquist curves of NSLPC and Pt/C catalyst are shown in Fig. 5f. The corresponding equivalent circuit (insert of Fig. 5f) consists of Rs, Rct, W and Cdl, which represent the electrolyte resistance, charge transfer resistance, electrolyte ions

diffusion resistance, constant phase elements of the double layer, respectively [65]. Clearly, the Rct value of NSLPC (39.4 Ω) is smaller than that of Pt/C catalyst (47.6 Ω) in the Nyquist plot, demonstating a lower resistance at NSLPC-electrolyte interface than that at Pt/C-electrolyte interface.

4. Conclusions

In summary, the bifunctional NSLPC material is prepared by pyrolyzing the mixture of mulberry leaves, KOH and thiourea in Ar atmosphere, which possesses abundant micropores, mesopores, proper content of doped N,S species and high surface area. In terms of SC, the NSLPC sample presents a specific capacitance of 243.4 F g^{-1} at 0.1 A g^{-1} and 214.5 F g^{-1} at 0.5 A g^{-1} and excellent durability with 94 % retention at 3 A g^{-1} after 5000 cycles in SCs. On the other hand, for ORR, the NSLPC sample exhibits outstanding stability and also overcomes the poor resistance to methanol cross-over compared to commercial Pt/C catalyst. In conclusion, the excellent SC and ORR performance indicates that NSLPC is a prospective candidate materials for electrochemical application.

Acknowledgements.

This study was financially supported by National Key R&D program of China (2017YFB0305600) and National Natural Science Foundation of China (Grant No.51471054).

References

[1] J. Yan, Q. Wang, T. Wei, Z. Fan, Recent advances in design and fabrication of electrochemical supercapacitors with high Energy densities, Adv. Energy Mater. 4 (2014) 1300816.

[2] S. Gao, X. Li, L. Li, X. Wei, A versatile biomass derived carbon material for oxygen reduction reaction, supercapacitors and oil/water separation, Nano Energy 33 (2017) 334-342.

[3] Z.S. Wu, S. Yang, Y. Sun, K. Parvez, X. Feng, K. Muellen, 3D nitrogen-doped graphene aerogel-supported Fe_3O_4 nanoparticles as efficient eletrocatalysts for the oxygen reduction reaction, J. Am. Chem. Soc. 134 (2012) 9082-9085.

[4] K. Gong, F. Du, Z. Xia, M. Durstock, L. Dai, Nitrogen-doped carbon nanotube arrays with high electrocatalytic activity for oxygen reduction, Science 323 (2009) 760-764.

[5] M. Zhang, X. Jin, L. Wang, M. Sun, Y. Tang, Y. Chen, Y. Sun, X. Yang, P. Wan, Improving biomass-derived carbon by activation with nitrogen and cobalt for supercapacitors and oxygen reduction reaction, Appl. Surf. Sci. 411 (2017) 251-260.

[6] J. Xu, Z.Q. Tan, W.C. Zeng, G.X. Chen, S.L. Wu, Y. Zhao, K. Ni, Z.C. Tao, M. Ikram, H.X. Ji, Y.W. Zhu, A hierarchical carbon derived from sponge-templated activation of graphene oxide for high-performance supercapacitor electrodes, Adv. Mater. 28 (2016) 5222-5228.

[7] X. Zhang, J.M. Wang, J. Liu, J. Wu, H. Chen, H. Bi, Design and preparation of a ternary composite of graphene oxide/carbon dots/polypyrrole for supercapacitor application: Importance and unique role of carbon dots, Carbon 115 (2017) 134-146.

[8] D. Yu, X. He, 3D cobalt-embedded nitrogen-doped graphene xerogel as an efficient electrocatalyst for oxygen reduction reaction in an alkaline medium, J. Appl. Electrochem. 47 (2016) 13-23.

[9] Y. Cheng, S. Lu, H. Zhang, C.V. Varanasi, J. Liu, Synergistic effects from graphene and carbon nanotubes enable flexible and robust electrodes for high-performance supercapacitors, Nano Lett. 12 (2012) 4206-4211.

[10] W. Xiong, F. Du, Y. Liu, A. Perez, Jr., M. Supp, T.S. Ramakrishnan, L. Dai, L. Jiang, 3-D Carbon Nanotube Structures Used as High Performance Catalyst for Oxygen Reduction Reaction, J. Am. Chem. Soc. 132 (2010) 15839-15841.

[11] G.L. Tian, M.Q. Zhao, D.S. Yu, X.Y. Kong, J.Q. Huang, Q. Zhang, F. Wei, Nitrogen-doped graphene/carbon nanotube hybrids: in situ formation on bifunctional catalysts and their superior electrocatalytic activity for oxygen evolution/reduction reaction, Small 10 (2014) 2251-2259.

[12] S.A. Wohlgemuth, R.J. White, M.G. Willinger, M.M. Titirici, M. Antonietti, A one-pot hydrothermal synthesis of sulfur and nitrogen doped carbon aerogels with enhanced electrocatalytic activity in the oxygen reduction reaction, Green Chem. 14 (2012) 1515-1523.

[13] Q.T. Qu, Y. Shi, S. Tian, Y.H. Chen, Y.P. Wu, R. Holze, A new cheap asymmetric aqueous supercapacitor: activated carbon/$NaMnO_2$, J. Power Sources 194 (2009) 1222-1225.

[14] Y. Li, G. Wang, T. Wei, Z. Fan, P. Yan, Nitrogen and sulfur co-doped porous carbon nanosheets derived from willow catkin for supercapacitors, Nano Energy 19 (2016) 165-175.

[15] L.J. Zhang, Z.X. Su, F.L. Jiang, L.L. Yang, J.J. Qian, Y.F. Zhou, W.M. Li, M.C. Hong, Highly graphitized nitrogen-doped porous carbon nanopolyhedra derived from ZIF-8 nanocrystals as efficient electrocatalysts for oxygen reduction reactions, Nanoscale 6 (2014) 6590-6602.

[16] H. Yu, L. Shang, T. Bian, R. Shi, G.I. Waterhouse, Y. Zhao, C. Zhou, L.Z. Wu, C.H. Tung, T. Zhang, Nitrogen-doped porous carbon nanosheets templated from g-C_3N_4 as metal-free electrocatalysts for efficient oxygen reduction reaction, Adv. Mater. 28 (2016) 5080-5086.

[17] Y.J. Chen, S.F. Ji, Y.G. Wang, J.C. Dong, W.X. Chen, Z. Li, R.A. Shen, L.R. Zheng, Z.B. Zhuang, D.S. Wang, Y.D. Li, Isolated single iron atoms anchored on N-doped porous carbon as an efficient electrocatalyst for the oxygen reduction reaction, Angew. Chem. 56 (2017) 6937-6941.

[18] X. Chen, J. Zhang, B. Zhang, S. Dong, X. Guo, X. Mu, B. Fei, A novel hierarchical porous nitrogen-doped carbon derived from bamboo shoot for high performance supercapacitor, Sci. Rep. 7 (2017) 7362.

[19] D. Zhu, J. Jiang, D. Sun, X. Qian, Y. Wang, L. Li, Z. Wang, X. Chai, L. Gan, M. Liu, A general strategy to synthesize high-level N-doped porous carbons via Schiff-base chemistry for supercapacitors, J. Mater. Chem. A 6 (2018) 12334-12343.

[20] Z. Song, D. Zhu, D. Xue, J. Yan, X. Chai, W. Xiong, Z. Wang, Y. Lv, T. Cao, M. Liu, L. Gan, N-enriched hollow porous carbon nanospheres with tailored morphology and microstructure for all-solid-state symmetric supercapacitors, ACS Appl. Energy Mater. 1 (2018) 4293-4303.

[21] J.J. Li, Y.M. Zhang, X.H. Zhang, J.Z. Huang, J.C. Han, Z.H. Zhang, X.J. Han, P. Xu, B. Song, S, N dual-doped graphene-like carbon nanosheets as efficient oxygen reduction reaction electrocatalysts, ACS Appl. Mater. Interfaces 9 (2017) 398-405.

[22] T. Wang, L.X. Wang, D.L. Wu, W. Xia, D.Z. Jia, Interaction between nitrogen and sulfur in co-doped graphene and synergetic effect in supercapacitor, Sci. Rep. 5 (2015) 9591.

[23] L. Miao, D. Zhu, M. Liu, H. Duan, Z. Wang, Y. Lv, W. Xiong, Q. Zhu, L. Li, X. Chai, L. Gan, Cooking carbon with protic salt: nitrogen and sulfur self-doped porous carbon nanosheets for supercapacitors, Chem. Eng. J. 347 (2018) 233-242.

[24] Y. Li, S. Lin, X. Ren, H. Mi, P. Zhang, L. Sun, L. Deng, Y. Gao, One-step rapid in-situ synthesis of nitrogen and sulfur co-doped three-dimensional honeycomb-ordered carbon supported PdNi nanoparticles as efficient electrocatalyst for oxygen reduction reaction in alkaline solution, Electrochim. Acta 253 (2017) 445-454.

[25] G. Xu, J. Han, B. Ding, P. Nie, J. Pan, H. Dou, H. Li, X. Zhang, Biomass-derived porous carbon materials with sulfur and nitrogen dual-doping for energy storage, Green Chem. 17 (2015) 1668-1674.

[26] N. Sudhan, K. Subramani, M. Karnan, N. Ilayaraja, M. Sathish, Biomass-derived activated porous carbon from rice straw for a high-energy symmetric supercapacitor in aqueous and non-aqueous electrolytes, Energy Fuels 31 (2017) 977-985.

[27] K. Chaitra, R.T. Vinny, P. Sivaraman, N. Reddy, C. Hu, K. Venkatesh, C.S. Vivek, N. Nagaraju, N. Kathyayini, KOH activated carbon derived from biomass-banana fibers as an efficient negative electrode in high performance asymmetric supercapacitor, J. Energy Chem. 26 (2017) 56-62.

[28] G. Ma, Q. Yang, K. Sun, H. Peng, F. Ran, X. Zhao, Z. Lei, Nitrogen-doped porous carbon derived from biomass waste for high-performance supercapacitor, Bioresour. Technol. 197 (2015) 137-142.

[29] X. Wu, S. Li, B. Wang, J. Liu, M. Yu, From biomass chitin to mesoporous nanosheets assembled loofa sponge-like N-doped carbon/g-C_3N_4 3D network architectures as ultralow-cost bifunctional oxygen catalysts, Microporous Mesoporous Mater. 240 (2017) 216-226.

[30] P. Chen, L.-K. Wang, G. Wang, M.-R. Gao, J. Ge, W.-J. Yuan, Y.-H. Shen, A.-J. Xie, S.-H. Yu, Nitrogen-doped nanoporous carbon nanosheets derived from plant biomass: an efficient catalyst for oxygen reduction reaction, Energy Environ. Sci. 7 (2014) 4095-4103.

[31] H. Zhu, J. Yin, X. Wang, H. Wang, X. Yang, Microorganism-derived heteroatom-doped carbon materials for oxygen reduction and supercapacitors, Adv. Funct. Mater. 23 (2013) 1305-1312.

[32] J. Wang, S. Kaskel, KOH activation of carbon-based materials for energy storage, J. Mater. Chem. 22 (2012) 23710.

[33] J. Liu, X. Wang, Q. Lu, R. Yu, M. Chen, S. Cai, X. Wang, Synthesis of nitrogen and sulfur co-doped carbon derived from chromium carbide for the high performance supercapacitor, J. Electrochem. Soc. 163 (2016) A2991-A2998.

[34] J. Chmiola, G. Yushin, Y. Gogotsi, C. Portet, P. Simon, P.L. Taberna, Anomalous increase in carbon capacitance at pore sizes less than 1 nanometer, Science 313 (2006) 1760-1763.

[35] Y. Zhao, M. Liu, L. Gan, X. Ma, D. Zhu, Z. Xu, L. Chen, Ultramicroporous Carbon Nanoparticles for the High-Performance Electrical Double-Layer Capacitor Electrode, Energy Fuels 28 (2014) 1561-1568.

[36] M. Liu, J. Qian, Y. Zhao, D. Zhu, L. Gan, L. Chen, Core–shell ultramicroporous@microporous carbon nanospheres as advanced supercapacitor electrodes, J. Mater. Chem. A 3 (2015) 11517-11526.

[37] W. Lu, M. Liu, L. Miao, D. Zhu, X. Wang, H. Duan, Z. Wang, L. Li, Z. Xu, L. Gan, L. Chen, Nitrogen-containing ultramicroporous carbon nanospheres for high performance supercapacitor electrodes, Electrochim. Acta 205 (2016) 132-141.

[38] L. Miao, H. Duan, M. Liu, W. Lu, D. Zhu, T. Chen, L. Li, L. Gan, Poly(ionic liquid)-derived, N, S-codoped ultramicroporous carbon nanoparticles for supercapacitors, Chem. Eng. J. 317 (2017) 651-659.

[39] J. Zhu, D. Xu, C. Wang, W. Qian, J. Guo, F. Yan, Ferric citrate-derived N-doped hierarchical porous carbons for oxygen reduction reaction and electrochemical supercapacitors, Carbon 115 (2017) 1-10.

[40] D. Zhang, L. Zheng, Y. Ma, L. Lei, Q. Li, Y. Li, H. Luo, H. Feng, Y. Hao, Synthesis of nitrogen- and sulfur-codoped 3D cubic-ordered mesoporous carbon with superior performance in supercapacitors, ACS Appl. Mater. Interfaces 6 (2014) 2657-2665.

[41] H.T. Yi, Y.Q. Zhu, X.Y. Chen, Z.J. Zhang, Nitrogen and sulfur co-doped nanoporous carbon material derived from p-nitrobenzenamine within several minutes and the supercapacitor application, J. Alloys Compd. 649 (2015) 851-858.

[42] C. Wang, T. Liu, Nori-based N, O, S, Cl co-doped carbon materials by chemical activation of $ZnCl_2$ for supercapacitor, J. Alloys Compd. 696 (2017) 42-50.

[43] T. Sharifi, G. Hu, X. Jia, T. Wagberg, Formation of active sites for oxygen reduction reactions by transformation of nitrogen functionalities in nitrogen-doped carbon nanotubes, ACS Nano 6 (2012) 8904-8912.

[44] Z. Yang, Z. Yao, G.F. Li, G.Y. Fang, H.G. Nie, Z. Liu, X.M. Zhou, X. Chen, S.M. Huang, Sulfur-doped graphene as an efficient metal-free cathode catalyst for oxygen reduction, ACS Nano 6 (2012) 205-211.

[45] L. Miao, D. Zhu, M. Liu, H. Duan, Z. Wang, Y. Lv, W. Xiong, Q. Zhu, L. Li, X. Chai, L. Gan, N, S Co-doped hierarchical porous carbon rods derived from protic salt: Facile synthesis for high energy density supercapacitors, Electrochim. Acta 274 (2018) 378-388.

[46] J. Liang, Y. Jiao, M. Jaroniec, S.Z. Qiao, Sulfur and nitrogen dual-doped mesoporous graphene electrocatalyst for oxygen reduction with synergistically enhanced performance, Angew. Chem. 51 (2012) 11496-11500.

[47] R.S. Mehare, S.P. Ranganath, V. Chaturvedi, M.V. Badiger, M.V. Shelke, In situ synthesis of nitrogen- and sulfur-enriched hierarchical porous carbon for high-performance supercapacitor, Energy Fuels 32 (2018) 908-915.

[48] T. Qin, Z. Wan, Z. Wang, Y. Wen, M. Liu, S. Peng, D. He, J. Hou, F. Huang, G. Cao, 3D flexible O/N Co-doped graphene foams for supercapacitor electrodes with high volumetric and areal capacitances, J. Power Sources 336 (2016) 455-464.

[49] M. Seredych, T.J. Bandosz, S-doped micro/mesoporous carbon-graphene composites as efficient supercapacitors in alkaline media, J. Mater. Chem. A 1 (2013) 11717-11727.

[50] J. Wei, D. Zhou, Z. Sun, Y. Deng, Y. Xia, D. Zhao, A controllable synthesis of rich nitrogen-doped ordered mesoporous carbon for CO_2 capture and supercapacitors, Adv. Funct. Mater. 23 (2013) 2322-2328.

[51] X. Qing, Y. Cao, J. Wang, J. Chen, Y. Lu, P/N/O co-doped carbonaceous material based supercapacitor with voltage up to 1.9 V in aqueous electrolyte, RSC Adv. 4 (2014) 55971-55979.

[52] X. Wang, Y. Li, F. Lou, M.E.M. Buan, E. Sheridan, D. Chen, Enhancing capacitance of supercapacitor with both organic electrolyte and ionic liquid electrolyte on a biomass-derived carbon, RSC Adv. 7 (2017) 23859-23865.

[53] P. Hao, Z. Zhao, Y. Leng, J. Tian, Y. Sang, R.I. Boughton, C.P. Wong, H. Liu, B. Yang, Graphene-based nitrogen self-doped hierarchical porous carbon aerogels derived from chitosan for high performance supercapacitors, Nano Energy 15 (2015) 9-23.

[54] X. He, P. Ling, J. Qiu, M. Yu, X. Zhang, C. Yu, M. Zheng, Efficient preparation of biomass-based mesoporous carbons for supercapacitors with both high energy density and high power density, J. Power Sources 240 (2013) 109-113.

[55] M. Chen, X. Kang, T. Wumaier, J. Dou, B. Gao, Y. Han, G. Xu, Z. Liu, L. Zhang, Preparation of activated carbon from cotton stalk and its application in supercapacitor, J. Solid State Electrochem. 17 (2012) 1005-1012.

[56] M.-C. Liu, L.-B. Kong, P. Zhang, Y.-C. Luo, L. Kang, Porous wood carbon monolith for high-performance supercapacitors, Electrochim. Acta 60 (2012) 443-448.

[57] V. Subramanian, C. Luo, A.M. Stephan, K.S. Nahm, S. Thomas, B.Q. Wei, Supercapacitors from activated carbon derived from banana fibers, J. Phys. Chem. C 111 (2007) 7527-7531.

[58] M. Olivares-Marín, J.A. Fernández, M.J. Lázaro, C. Fernández-González, A. Macías-García, V. Gómez-Serrano, F. Stoeckli, T.A. Centeno, Cherry stones as precursor of activated carbons for supercapacitors, Mater. Chem. Phys. 114 (2009) 323-327.

[59] L. Liu, S.D. Xu, Q. Yu, F.Y. Wang, H.L. Zhu, R.L. Zhang, X. Liu, Nitrogen-doped hollow carbon spheres with a wrinkled surface: their one-pot carbonization synthesis and supercapacitor properties, Chem. Commun. 52 (2016) 11693-11696.

[60] L. Wang, Z. Gao, J. Chang, X. Liu, D. Wu, F. Xu, Y. Guo, K. Jiang, Nitrogen-doped porous carbons as electrode materials for high-performance supercapacitor and dye-sensitized solar cell, ACS Appl. Mater. Interfaces 7 (2015) 20234-20244.

[61] E. Hao, W. Liu, S. Liu, Y. Zhang, H. Wang, S. Chen, F. Cheng, S. Zhao, H. Yang, Rich sulfur doped porous carbon materials derived from ginkgo leaves for multiple electrochemical energy storage devices, J. Mater. Chem. A 5 (2017) 2204-2214.

[62] Z. Wu, R. Liu, J. Wang, J. Zhu, W. Xiao, C. Xuan, W. Lei, D. Wang, Nitrogen and sulfur co-doping of 3D hollow-structured carbon spheres as an efficient and stable metal free catalyst for the oxygen reduction reaction, Nanoscale 8 (2016) 19086-19092.

[63] L.F. Lai, J.R. Potts, D. Zhan, L. Wang, C.K. Poh, C.H. Tang, H. Gong, Z.X. Shen, L.Y. Jianyi, R.S. Ruoff, Exploration of the active center structure of nitrogen-doped graphene-based catalysts for oxygen reduction reaction, Energy Environ. Sci. 5 (2012) 7936-7942.

[64] J. Duan, S. Chen, S. Dai, S.Z. Qiao, Shape control of Mn_3O_4 nanoparticles on nitrogen-doped graphene for enhanced oxygen reduction activity, Adv. Funct. Mater. 24 (2014) 2072-2078.

[65] H. Huang, X. Wei, S. Gao, Nitrogen-doped porous carbon derived from malachium aquaticum biomass as a highly efficient electrocatalyst for oxygen reduction reaction, Electrochim. Acta 220 (2016) 427-435.

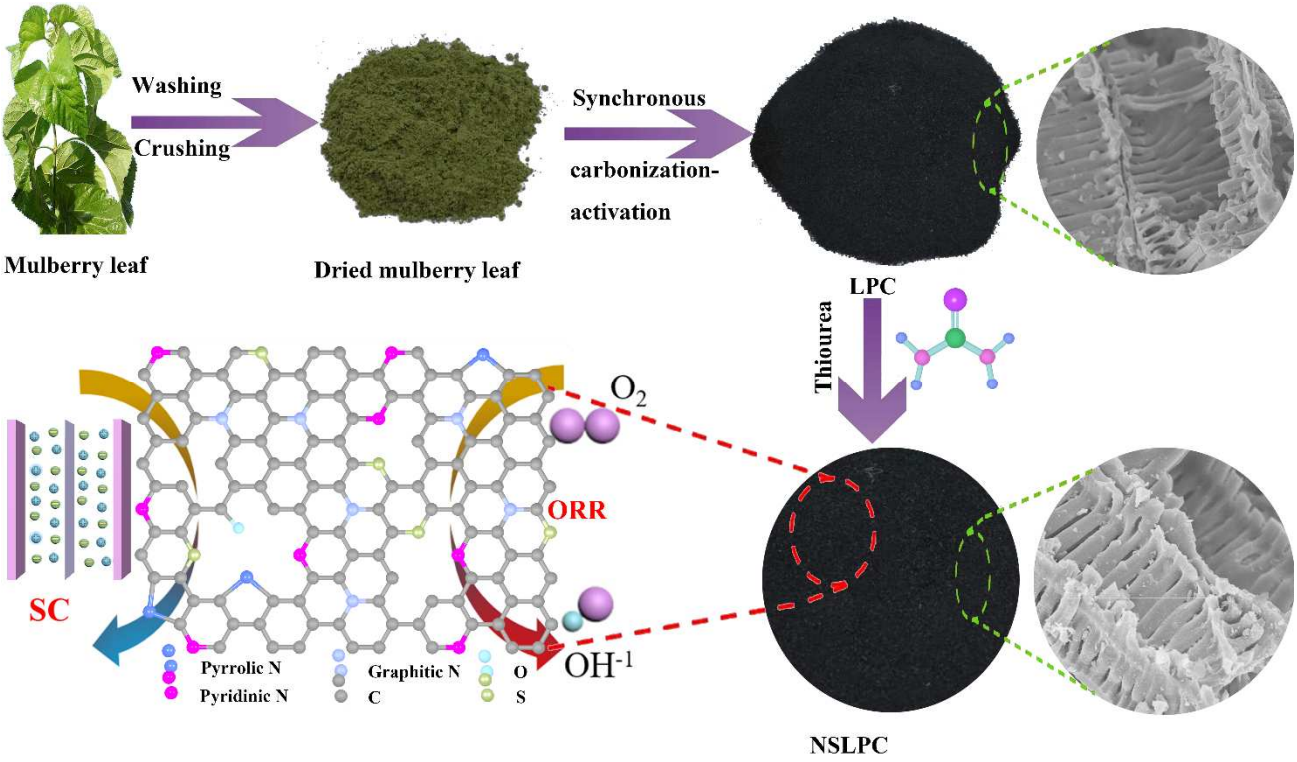

Scheme. 1. Schematic illustration for the synthesis route of NSLPC.

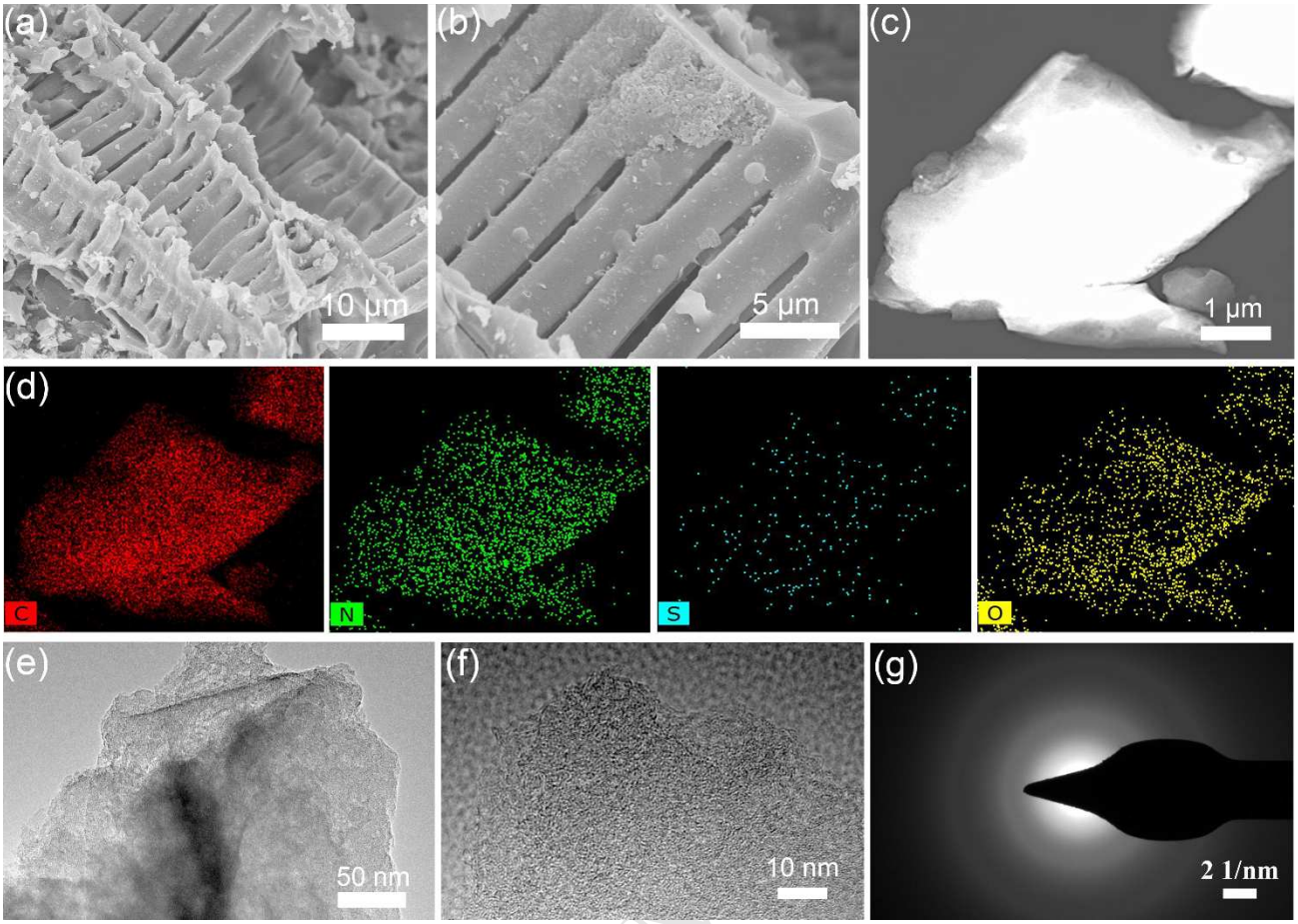

Fig. 1. The morphology and microstructure of the NSLPC sample: (a) low - and (b) high-magnification SEM images; (c) selected-area image of elemental mapping and (d) the corresponding EDS elemental mapping images; (e) TEM image, (f) HRTEM images and (g) the correspondings selected-area electron diffraction (SAED) pattern.

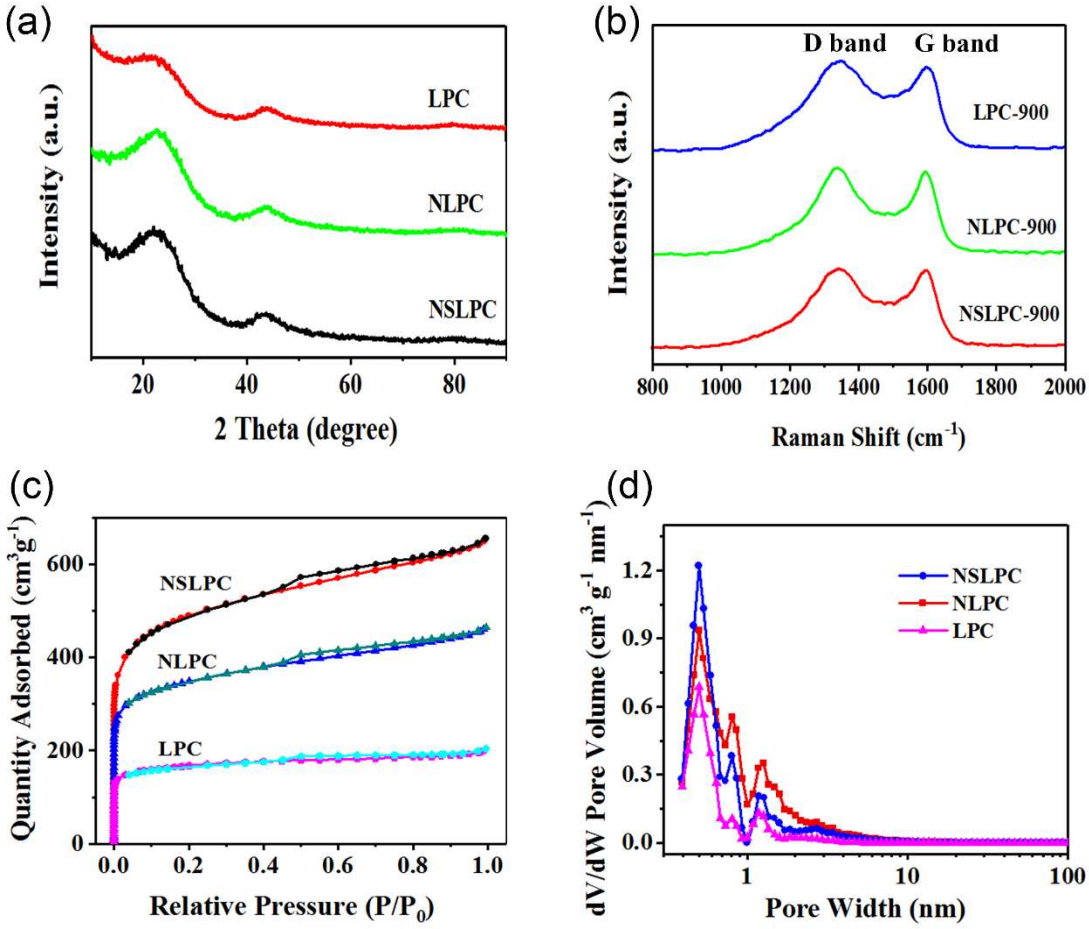

Fig. 2. (a) XRD patterns, (b) Raman spectra, (c) N_2 adsorption-desorption isotherms and (d) pore size distribution using density functional theory method of LPC, NLPC and NSLPC.

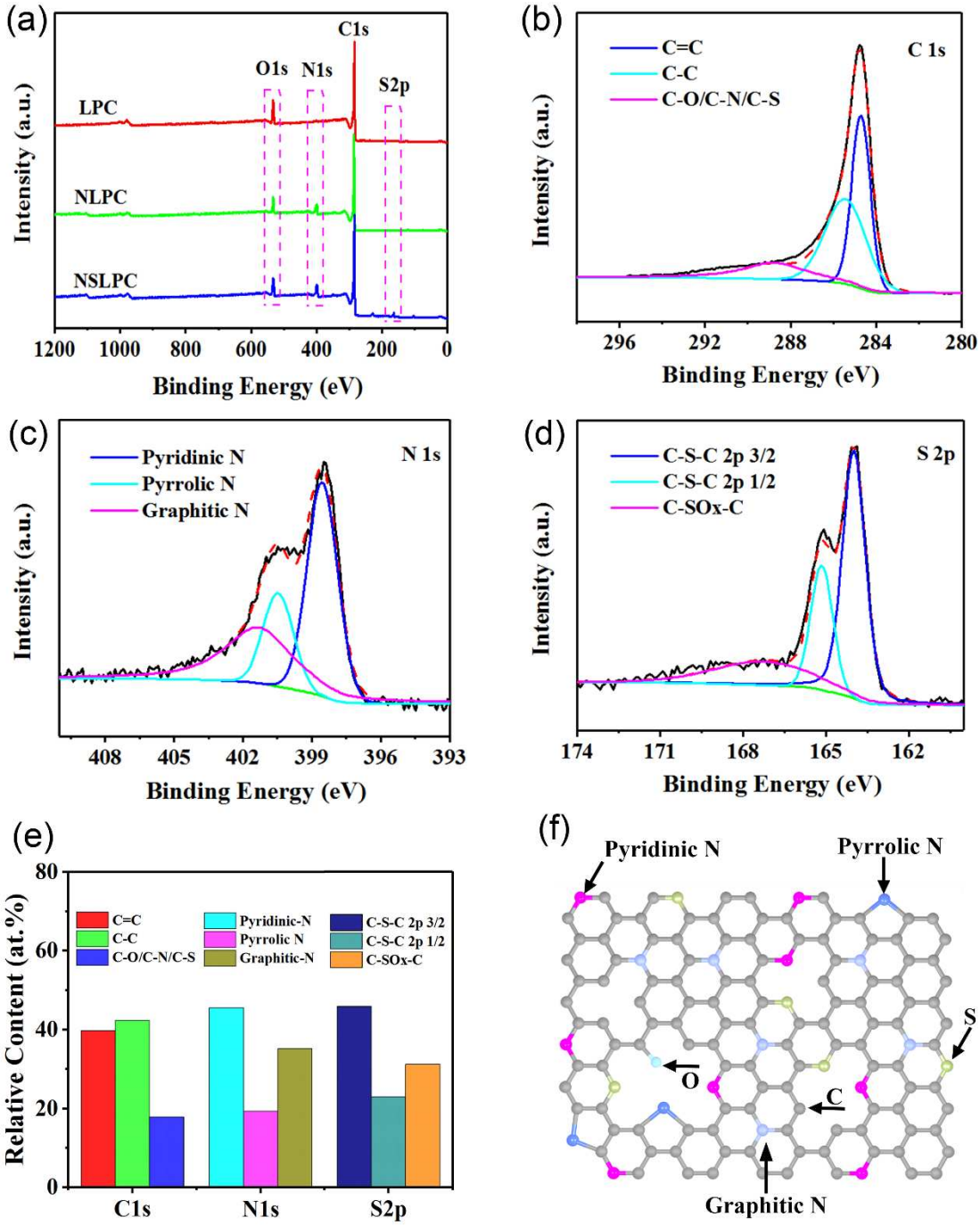

Fig. 3. XPS measurement on NSLPC: (a)XPS survey; high-resolution (b) C 1s, (c) N 1s and (d) S 2p; (e) the content of different atom species from the fitted data (C 1s, N 1s and S 2p); (f) schematic model for the chemical structure and possible distribution in carbon framework with nitrogen and sulfur dual-doping.

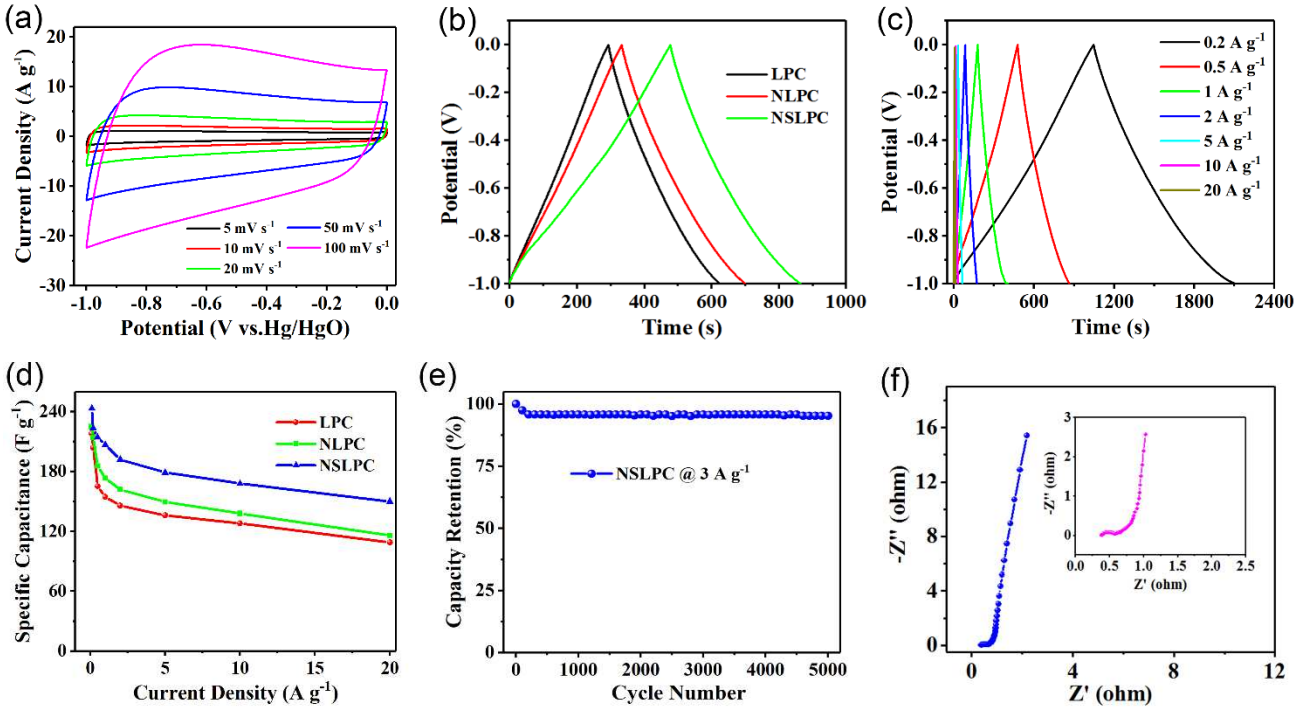

Fig. 4. (a) CV curves of NSLPC at various scan speed; (b) galvanostatic charge-discharge curves of LPC, NLPC and NSLPC at 0.5 A g^{-1}; (c) galvanostatic charge-discharge curves of NSLPC at different current densities; (d) specific capacitaces calculated from the discharge curves of LPC, NLPC and NSLPC at different current densities; (e) capacity retention of NSLPC at 3 A g^{-1}; (e) cycling stability a 20 A g^{-1}; (f) Nyquist plots of NSLPC in the frequency range of 10 mHz to 100 kHz.

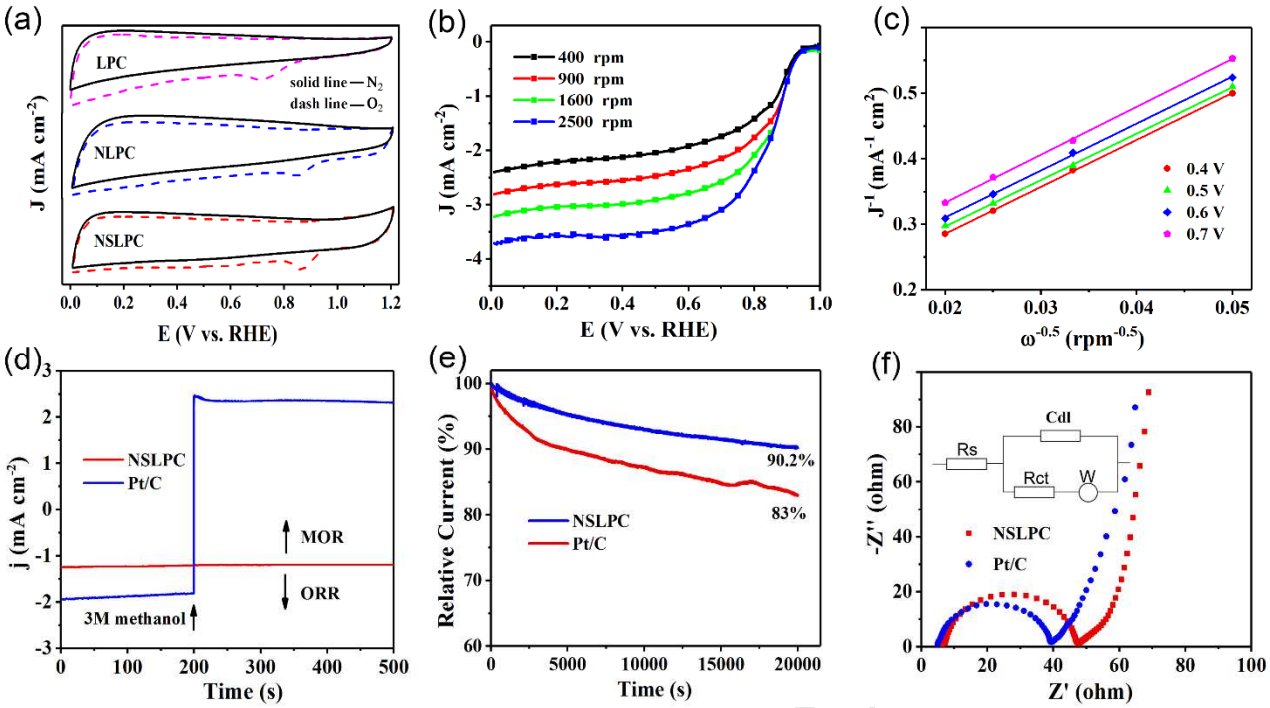

Fig. 5. (a) CV curves of LPC, NLPC and NSLPC in N_2-saturated (solid line) and O_2- saturated (dash line) 0.1 M KOH at a scan rate of 10 mV s^{-1}; (b) LSV curves of NSLPC with a sweep rate of 10 mV s^{-1} at different rotation speed; (c) corresponding K-L plots of NSLPC at different electrode potentials; (d) current-time (i-t) chronoamperometric responses at +0.7 V vs. RHE for NSLPC and Pt/C modified electrode with the addition of 3 M methanol in O_2-saturated 0.1 M KOH solution at 200 s; (e) stability evaluation of NSLPC and Pt/C for 20000 s at +0.7 V vs. RHE with a rotation speed of 900 rpm; (f) EIS of NSLPC and Pt/C at open potential (insert: equivalent circuit).

Table 1. Pore structure, BET and element contents of as-prepared samples.

Sample	S_{BET}[a]	V_{Total}[b]	V_{micro}[c]	$V_{meso+macro}$[d]	$D_{average}$[e]	XPS analysis (atom %)			
	(m^2 g^{-1})	(cm^3 g^{-1})	(cm^3 g^{-1})	(cm^3 g^{-1})	(nm)	C	N	O	S
LPC	568	0.315	0.209	0.106	2.21	89.61	0.7	9.7	-
NLPC	1207	0.717	0.318	0.399	2.37	84.95	8.11	6.94	-
NSLPC	1689	1.012	0.357	0.655	2.39	82.53	8.17	7.34	1.97

[a] Specific surface area calculated to BET (Brunauer-Emmett-Teller) method.

[b] Total pore volume.

[c] Micropore volume (V_{micro}) was calculated from the V-t plot.

[d] Meso/macropore volume ($V_{meso+macro}$) was acquired by subtracting V_{micro} from V_{Total}.

[e] Adsorption average pore diameter.

Table 2. Summary of electrochemical parameters of biomass/biowaste-derived carbon as supercapacitor electrodes compared with NSLPC

Carbon Precursor	SSA (m^2 g^{-1})	Electrolyte	Current density ($A \cdot g^{-1}$)	Specific Capacitance (F g^{-1})	Ref
Mulberry leaves	1689	6M KOH	0.1 0.2 0.5	243.4 223.4 214.5	this study
broad beans shell	655.4	6M KOH	0.5	202	[25]
chitosan	2435	6M KOH	0.2	197	[53]
peanut shell	1552	6M KOH	0.05	245	[54]
cotton stalk	1481	Et_4NBF_4	0.5	114	[55]
Poplar wood	467	2M KOH	0.3	234	[56]
banana fiber	1097	1 M Na_2SO_4	0.02	75	[57]
Cherry stones	1224	2 M H_2SO_4	0.05	230	[58]

Highlights

1. Mulberry leaves are used to prepare bifunctional carbon materials.
2. A unique ladder-like porous carbon is obtained for the first time.
3. The N,S doped porous carbon exhibits outstanding durability for SC.
4. The N,S doped porous carbon presents excellent long stability for ORR.